Interferometric ground-roll removal: Attenuation of scattered surface waves in single-sensor data (vol 75, pg SA15, 2010)

GEOPHYSICS, VOL. 75, NO. 2 (MARCH-APRIL 2010); P. SA15–SA25, 14 FIGS.
10.1190/1.3360948

Cite As: Halliday, DF, Curtis, A, Vermeer, P, Strobbia, C, Glushchenko, A, van Manen, D-J & Robertsson, JOA 2010, 'Interferometric ground-roll removal: Attenuation of scattered surface waves in single-sensor data (vol 75, pg SA15, 2010)' Geophysics, vol 75, no. 4, pp. Y1-Y1. DOI: 10.1190/1.3360948

Interferometric ground-roll removal: Attenuation of scattered surface waves in single-sensor data

David F. Halliday[1], Andrew Curtis[2], Peter Vermeer[3], Claudio Strobbia[3], Anna Glushchenko[3], Dirk-Jan van Manen[3], and Johan O. A. Robertsson[4]

ABSTRACT

Land seismic data are contaminated by surface waves (or ground roll). These surface waves are a form of source-generated noise and can be strongly scattered by near-surface heterogeneities. The resulting scattered ground roll can be particularly difficult to separate from the desired reflection data, especially when this scattered ground roll propagates in the crossline direction. We have used seismic interferometry to estimate scattered surface waves, recorded during an exploration seismic survey, between pairs of receiver locations. Where sources and receivers coincide, these interreceiver surface-wave estimates were adaptively subtracted from the data. This predictive-subtraction process can successfully attenuate scattered surface waves while preserving the valuable reflected arrivals, forming a new method of scattered ground-roll attenuation. We refer to this as interferometric ground-roll removal.

INTRODUCTION

In exploration seismology, surface waves (or ground roll) constitute a form of source-generated noise. Ground roll travels laterally through the near surface of the earth and contains little or no information about the deeper subsurface. These arrivals are characterized by a high amplitude and low-frequency content, and they often obscure recordings of body waves reflected by deeper subsurface targets. Conventionally, ground roll is removed using frequency-wavenumber (f-k) or frequency-offset (f-x) methods (e.g., Yilmaz, 2001). However, when near-surface heterogeneities cause ground roll to be scattered in the crossline direction, these conventional techniques can prove to be ineffective; crossline scattered ground roll can occupy the same regions of f-k and f-x space as the reflected waves that we wish to preserve.

Methods focusing on the removal of these scattered surface waves exist and can be separated into two categories: acquisition-based suppression schemes that are based on the use of recording arrays (e.g., Regone, 1998; Özbek, 2000), and prediction-removal suppression schemes that estimate and subtract scattered surface waves using either modeling-based (Blonk et al., 1995; Blonk and Herman, 1996; Ernst et al., 2002a; Ernst et al., 2002b) or data-driven (Herman and Perkins, 2006) inverse-scattering series. The use of extensive stacked arrays in acquisition-based schemes can compromise data resolution, and current prediction-removal schemes rely on time-consuming iterative inversions using the Born (single-scattering) approximation. In areas with strongly heterogeneous near-surface properties, a Born approximation might not be valid, and the inverse-scattering series might identify reflected waves as scattered events; hence these could be removed erroneously from the data.

In this study, we consider a prediction-removal suppression scheme that is based on the use of seismic interferometry (e.g., Wapenaar, 2003, 2004; van Manen et al., 2005, 2006; Curtis et al., 2006; Wapenaar and Fokkema, 2006) and adaptive filtering (e.g., Claerbout, 2004). This scheme is naturally applied to single-sensor data (because, for most purposes, seismic interferometry is naturally applied to single sensors), and it does not rely on array-based acquisition, single-scattering (Born) approximations, or the use of costly modeling and inversion processes. We show that this method is capable of removing complex and strongly scattered ground roll.

Interreceiver surface-wave signals can be estimated using seismic interferometry by performing a simple process of crosscorrelation (or crossconvolution) and summation of the wavefields observed at

Manuscript received by the Editor 26 June 2009; revised manuscript received 16 September 2009; published online 9 April 2010.
[1]Formerly University of Edinburgh, School of GeoSciences, Edinburgh, U. K., and Edinburgh Collaborative of Subsurface Science and Engineering (ECOSSE), U. K.; presently Schlumberger Cambridge Research, Cambridge, U. K. E-mail: DHalliday@slb.com.
[2]University of Edinburgh, School of GeoSciences, Edinburgh, U. K., and Edinburgh Collaborative of Subsurface Science and Engineering (ECOSSE), U. K. E-mail: Andrew.Curtis@ed.ac.uk.
[3]WesternGeco, Gatwick, U. K. E-mail: Vermeer@slb.com, cstrobbia@slb.com, aglushchenko1@slb.com, DManen@slb.com.
[4]Schlumberger Cambridge Research, Cambridge, U. K. E-mail: JRobertsson@slb.com.

the receivers (for crosscorrelation, see Wapenaar, 2003; van Manen et al., 2005; Wapenaar et al., 2006; and for crossconvolution, see Slob and Wapenaar, 2007; Slob et al., 2007). The main requirement is that sources excite the recorded wavefields from a suitable range of directions. We find that when sources are located only at the surface of the earth, estimates are dominated by surface waves. This dominance of surface waves is observed in passive seismology (Shapiro and Campillo, 2004; Shapiro et al., 2005; Gerstoft et al., 2006), in near-surface (engineering) seismology (Chávez-García and Luzón, 2005; Halliday et al., 2008), and in exploration seismology (Dong et al., 2006; Halliday et al., 2007; Vasconcelos et al., 2008). Note that Halliday et al. (2008) also show that the dispersive properties of multimode surface waves can be estimated using active source interferometry.

If each source location within an exploration survey is located near a receiver position, then surface-wave estimates can be created for each source-receiver pair. These estimates can be adaptively subtracted from the directly recorded full wavefield. We refer to this technique as interferometric ground-roll removal.

Interferometric ground-roll removal has received some attention in the literature. Previous studies consider surface waves propagating directly between receiver locations in numerical and real-data studies (Curtis et al., 2006; Dong et al., 2006; Halliday et al., 2007) and show the method to be effective for these direct surface waves. Although Vasconcelos et al. (2008) consider in-line scattered surface waves in their study, and Halliday and Curtis (2009) present a theoretical study of scattered surface-wave interferometry, no successful application has been published for crossline scattered surface waves recorded in a real exploration setting. Although it is desirable to be able to produce estimates using recordings of background noise, for the ground-roll removal application we require the bandwidth of the estimates to match those of the active source data. The only way to ensure this is to use active source data, because we cannot guarantee that background-noise sources will excite the frequencies of interest (e.g., Halliday et al., 2008, show that in one particular setting, the results of passive interferometry are dominated by a lower-frequency content than active source data).

In this paper, we first review interferometric theory for scattered waves and develop a workflow for the prediction of scattered surface waves by seismic interferometry. We then introduce a subset of a single-sensor land seismic survey wherein we observe strong lateral scattering. We apply both correlation-type and convolution-type interferometry to these data and illustrate the adaptive subtraction of scattered surface-wave estimates from the appropriate source-receiver recordings. Finally, we show how the two approaches might be combined to allow the method to be applied to an entire shot gather, and hence the method can be used as part of a conventional seismic processing flow.

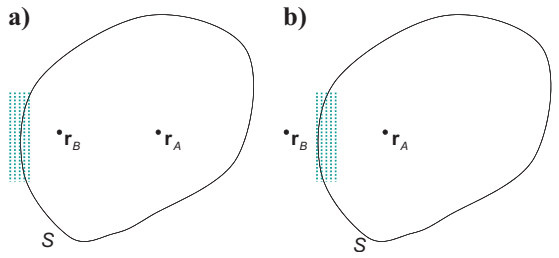

Figure 1. Configurations for (a) correlation-type interferometry and (b) convolution-type interferometry. In practice, it is not possible to form enclosing source boundaries S as shown here. Instead, portions of the source boundary can be formed using available source distributions. Green squares indicate distributions of sources that could replace the surface integral in practice.

SEISMIC INTERFEROMETRY: SCATTERED SURFACE-WAVE ISOLATION

Seismic interferometry is applied by evaluating a so-called interferometric integral. Such an integral requires integration across a bounding surface of sources S. In their most complicated form, interferometric integrals require that various source types exist on the bounding surfaces. For example, where the bounding surface does not coincide with a real surface or interface (e.g., the earth's free surface), the integrals require point forces and their spatial derivatives. However, because in practice source types are limited, we can use approximations to reduce these integrals to more practical forms.

For example, Wapenaar and Fokkema (2006) reduce the interferometric integral to include a summation over P- and S-wave sources by assuming that the surface S is a sphere with a large radius and that the medium at and around the surface is homogeneous. Further, for surface waves, Halliday and Curtis (2008) show that it is reasonable to replace these P- and S-wave sources with point forces; i.e., in the frequency domain

$$G^*_{im}(\mathbf{r}_B,\mathbf{r}_A) - G_{im}(\mathbf{r}_B,\mathbf{r}_A) \approx \frac{C(\omega)}{|S(\omega)|^2}\int_{\mathbf{r}_S\in S} G_{in}(\mathbf{r}_B,\mathbf{r}_S) \times G^*_{mn}(\mathbf{r}_A,\mathbf{r}_S)dS, \quad (1)$$

where $G_{im}(\mathbf{r}_B,\mathbf{r}_A)$ denotes the Green's function representing the ith component of particle displacement at location $\mathbf{r}_B$ due to a unidirectional, impulsive, point force in the m-direction at $\mathbf{r}_A$; the superscript * denotes complex conjugation; and the surface S encloses the locations $\mathbf{r}_A$ and $\mathbf{r}_B$ (see Figure 1a). Einstein's summation convention applies for repeat indices of source direction, and $S(\omega)$ is the source signature of the boundary sources.

The scale factor $C(\omega)$ occurs due to the approximations involved in relaxing the required source types. This scale factor can be related to frequency, the elastic properties at the source location, and the geometry of the source boundary (Wapenaar and Fokkema, 2006). On the left-hand side of equation 1, there are forward-time and reverse-time parts (complex conjugation in the frequency domain corresponds to time reversal). In practice, equation 1 is applied by summing over available source locations instead of solving an integral equation:

$$G^*_{im}(\mathbf{r}_B,\mathbf{r}_A) - G_{im}(\mathbf{r}_B,\mathbf{r}_A) \approx \frac{C(\omega)}{|S(\omega)|^2}\sum_S G_{in}(\mathbf{r}_B,\mathbf{r}_S)G^*_{mn}(\mathbf{r}_A,\mathbf{r}_S). \quad (2)$$

Finally, we assume that the vertical components dominate (as assumed for surface waves by Blonk et al., 1995):

$$G^*_{33}(\mathbf{r}_B,\mathbf{r}_A) - G_{33}(\mathbf{r}_B,\mathbf{r}_A) \approx \frac{C(\omega)}{|S(\omega)|^2}\sum_S G_{33}(\mathbf{r}_B,\mathbf{r}_S)G^*_{33}(\mathbf{r}_A,\mathbf{r}_S). \quad (3)$$

Equation 3 is similar to equation 5 of Bakulin and Calvert (2006), on which these authors base their virtual-source method. This equa-

tion uses only vertical point forces and measurements of vertical particle velocity, as is typical in land-seismic exploration using vibroseis sources and vertical-component geophones. It is likely that, by omitting the horizontal components, further amplitude errors will be introduced; however, we expect that the phase of the direct and scattered surface waves still can be adequately estimated. Bakulin and Calvert (2006) find that their results are reliable, despite the approximations required. For the surface-wave case, Dong et al. (2006), Halliday et al. (2007), and Halliday et al. (2008) consider only vertical force sources and find that their (direct) surface-wave estimates are reliable. We expect that such source types also can produce estimates of scattered surface waves.

The theory of correlation-type interferometry (as represented by equations 1–3) dictates that the medium through which the waves propagate must be lossless. The presence of losses can introduce amplitude errors and nonphysical arrivals into the interferometric estimates (Draganov et al., 2010). Interferometry can also be applied using convolution. This approach places no restrictions on the attenuation properties of the medium (Slob and Wapenaar, 2007; Slob et al., 2007; Wapenaar, 2007; Halliday and Curtis, 2009), and we expect convolution applications to be less sensitive to nonphysical arrivals introduced by attenuation and limited aperture.

Halliday and Curtis (2009) show why the convolution results are better than the results of using correlation when trying to estimate scattered surface waves. Their stationary-phase analysis reveals that there are mutually canceling contributions in correlation-type interferometry that do not exist in convolution-type interferometry. When interferometry is applied in attenuative media or with limited aperture (or indeed both), the mutual cancellation might not necessarily occur, and artifacts (nonphysical wave energy) are introduced into the interferometric estimates. This effect has been observed also for acoustic scattering (Snieder et al., 2008) and for reflected wavefields (Draganov et al., 2010).

For this convolution case, we simply remove the complex conjugate from equation 3,

$$G_{33}(\mathbf{r}_B,\mathbf{r}_A) \approx \frac{C(\omega)}{S(\omega)S(\omega)} \sum_S G_{33}(\mathbf{r}_B,\mathbf{r}_S) G_{33}(\mathbf{r}_A,\mathbf{r}_S), \quad (4)$$

and require that one of the receivers be located outside the boundary of sources (i.e., we require that the interreceiver line is dissected by the boundary of sources, Figure 1b). We have included the source signatures for completeness; in practice, we do not estimate these but instead allow the least-squares filtering process to account for them. Note that Poletto and Farina (2008) and Poletto and Wapenaar (2009) show that an equation similar to equation 4 (but applied with a different geometry) can be used to synthesize virtual reflections.

In the following, we assume that the surface waves propagate in two dimensions across the surface of the earth, and therefore we consider only sources and receivers located on (or just below) the free surface. Halliday and Curtis (2008) show that surface-wave estimates can be made using such source geometries, provided that no strong higher modes exist (or by isolating each mode and applying interferometry to the individual modes). By splitting the surface waves into direct and scattered parts, Halliday and Curtis (2009) apply a stationary-phase analysis and find that the scattered surface waves can be estimated by correlating (or convolving) the direct surface waves at the virtual source, with the scattered surface waves at the second receiver. (Stationary-phase analysis assumes that the major contributions to an integral come from those points at which the phase of the integral is stationary; by applying this method to seismic interferometry, it is possible to locate those regions of the surface S from which the major contributions to interferometry come).

For the separation of wavefields, similar results have been found for acoustic wave propagation by Snieder et al. (2008) and Vasconcelos et al. (2009). Poletto and Farina (2008) also consider stationary-phase analysis for the application of equations similar to equations 3 and 4 above. In the crosscorrelation case, those studies show that nonphysical (or spurious) arrivals can be introduced when crosscorrelating only direct and scattered waves, and these might be accentuated by the presence of attenuation.

For each source on the boundary S, we separate the surface-wave signals into two parts, one approximating the direct surface waves $G^{\mathrm{d}}_{33}(\mathbf{r}_A,\mathbf{r}_S)$, and another approximating the scattered surface waves $G^{\mathrm{sc}}_{33}(\mathbf{r}_A,\mathbf{r}_S)$. In this study, we use a combination of f-k filtering and time windowing to perform this separation; however, any other appropriate signal-processing technique could be used. As discussed above and in Halliday and Curtis (2009), we then can consider the application of interferometric equations of the form

$$\tilde{G}^{\mathrm{sc}*}_{33}(\mathbf{r}_B,\mathbf{r}_A) - \tilde{G}^{\mathrm{sc}}_{33}(\mathbf{r}_B,\mathbf{r}_A) \approx \sum_S G^{\mathrm{d}}_{33}(\mathbf{r}_B,\mathbf{r}_S) G^{\mathrm{sc}*}_{33}(\mathbf{r}_A,\mathbf{r}_S) + \sum_S G^{\mathrm{sc}}_{33}(\mathbf{r}_B,\mathbf{r}_S) G^{\mathrm{d}*}_{33}(\mathbf{r}_A,\mathbf{r}_S), \quad (5)$$

and

$$\tilde{G}^{\mathrm{sc}}_{33}(\mathbf{r}_B,\mathbf{r}_A) \approx \sum_S G^{\mathrm{d}}_{33}(\mathbf{r}_B,\mathbf{r}_S) G^{\mathrm{sc}}_{33}(\mathbf{r}_A,\mathbf{r}_S) + \sum_S G^{\mathrm{sc}}_{33}(\mathbf{r}_B,\mathbf{r}_S) G^{\mathrm{d}}_{33}(\mathbf{r}_A,\mathbf{r}_S), \quad (6)$$

for crosscorrelation and crossconvolution, respectively.

Note that the scattered surface-wave Green's function components on the left-hand side of equations 5 and 6 are estimates that might contain both physical and nonphysical events, and we have included the scale factor $C(\omega)$ and source term $S(\omega)$ within these Green's function estimates (cf. equation 3). We differentiate these from the exact scattered surface-wave component of the Green's function by using a tilde ($\sim$). In practice, we do not make estimates of the scattered surface waves on the right-hand side of equations 5 and 6. Instead, we make a "best guess" of the scattered waves by removing the direct surface waves and time windowing the earlier arrivals, resulting in an estimate of the scattered surface waves that also includes body-wave arrivals. This process is discussed in more detail below.

Note that equations 5 and 6 are very similar to equations 16 and 21 of Vasconcelos et al. (2009). Although we have derived these equations using observations from a stationary-phase analysis, those authors derive similar expressions for acoustic wave propagation using representation theorems for perturbed media. Similar wavefield-separation techniques are proposed and used successfully by Mehta et al. (2007) and Vasconcelos and Snieder (2008). In practice, it is unlikely that the available sources will form a closed boundary; nevertheless, we can select sources to be considered in the same manner

as these boundary sources. For example, in the following we consider a thick boundary of sources concentrated around the interreceiver line (indicated by the areas of gray squares in Figure 1).

In the results presented here, we consider only the application of one of the summations on the right-hand side of equations 5 and 6. We isolate the direct surface waves at the virtual source and cross-correlate or crossconvolve these estimates with the isolated scattered waves at the second receiver. In the specific case that we consider, we find that the other summation does not contribute to the scattered surface-wave estimate. This is likely to be due to the combination of the specific source, receiver, and scattering geometries considered here, and this might not necessarily be the case in other data sets.

DATA SET GEOMETRY AND PREPROCESSING FOR INTERFEROMETRY

We use a subset of single-sensor single-source data that was recorded as part of a test line in a desert. This subset consists of eight parallel lines of single-sensor receiver stations and nine parallel lines of vibroseis source stations (Figure 2). The eight receiver lines have a crossline separation of 6.25 m and an in-line receiver separation of 12.5 m (in a staggered pattern, sketched in the inset in Figure 2). The nine source lines have a crossline and an in-line separation of 25 m. The data themselves consist of 6-s records of correlated vibrator data, sampled at 4 ms. Apart from the vibroseis correlation, preprocessing also includes the application of a noise-attenuation algorithm, which uses a spatial median filter to identify anomalous amplitudes.

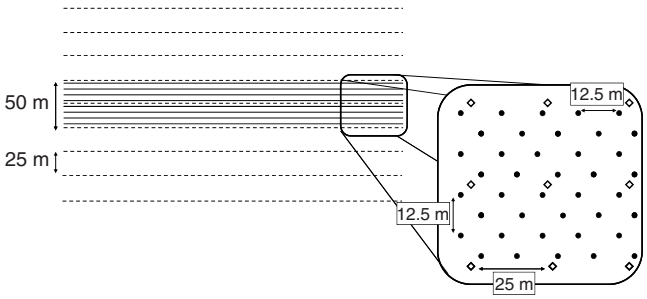

Figure 2. Sketch of the survey geometry. Dashed lines indicate source lines; solid lines indicate receiver lines. Inset shows source (diamond) and receiver (circle) geometries.

The data set is recorded in an area with a relatively strongly varying near surface (topographic and lithologic variations), and clear scattered ground-roll arrivals can be identified. In many parts of the data, strong in-line (i.e., linear) and crossline (i.e., hyperbolic) scattered surface-wave arrivals can be identified. For example, in Figure 3 we show an example of a particularly strong crossline scattered ground roll (about 1.5 s).

To apply interferometry to isolate the scattered surface waves, we require estimates of the separated wavefields $G_{33}^{\mathrm{d}}(\mathbf{r}_A,\mathbf{r}_S)$ and $G_{33}^{\mathrm{sc}}(\mathbf{r}_B,\mathbf{r}_S)$. This approximate separation of wavefields has two advantages: it allows us to apply interferometry in the framework laid out for the estimation of only scattered events (equations 5 and 6), and the preprocessing steps remove as much body-wave data from the recording as possible. Therefore this can also be considered to be a signal-preservation procedure. We apply the following workflow to estimate the interreceiver surface waves:

- Isolate the direct surface waves using a combination of f-k or f-x methods and time windowing.
- Remove any data that we can identify as not being a scattered surface wave; i.e., remove the direct surface-wave estimate from the data and zero any arrivals prior to the first arrival time of the direct surface wave.
- Select appropriate source geometries and apply either equation 5 or equation 6.

We choose a receiver as the virtual source location and show the source gather from the closest source to this receiver in Figure 3a. To begin processing the data using interferometry, as described above, we make estimates of the direct surface wave and the scattered surface waves. We apply a 1-Hz to 30-Hz band-pass filter to the data, because this is the frequency band in which the surface waves are dominant. The direct surface waves separated by using f-k filters and time windowing are shown in Figure 3b. We then remove the direct surface wave from the full-wavefield data (Figure 3c) and set the data equal to zero prior to the first surface-wave arrival (Figure 3d).

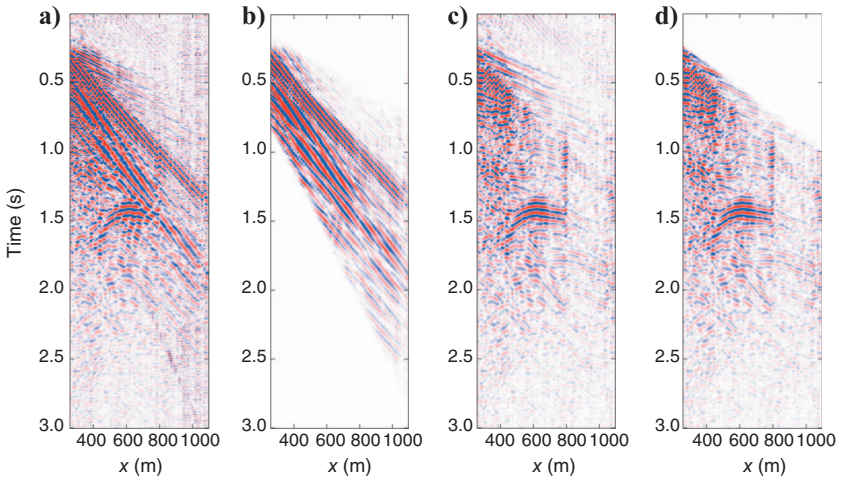

Figure 3. (a) Selection of a raw gather from the central source line and receiver line, recorded on the fifth receiver line; (b) direct surface waves isolated using f-k filtering and time windowing; (c) removal of (b) from (a) after band-pass filtering; and (d) zeroing of early arrivals in (c). The horizontal axis shows the source-receiver distance in meters. This and all subsequent x-axes are interpolated by a factor of four to smooth the plots.

The data in Figure 3b and d are representative of the data we use as the input to the interferometric estimation (i.e., these are estimates of $G_{33}^{\mathrm{d}}(\mathbf{r}_A,\mathbf{r}_S)$ and $G_{33}^{\mathrm{sc}}(\mathbf{r}_B,\mathbf{r}_S)$, respectively). This is the first step in our interferometric estimation process, and this step is repeated for all sources chosen to be treated as boundary sources. These preprocessing steps are similar to those used by Herman and Perkins (2006). However, instead of using an interferometric approach such as that illustrated here, those authors use an inversion-based approach to estimate a scattering distribution.

COMPARISON OF APPROACHES: CORRELATION OR CONVOLUTION?

In the section headed "Seismic interferometry: Scattered surface-wave isolation," we discussed the differences between the application of correlation-type interferometry and convolution-type interferometry. We now consider the application of both methods to estimate scattered surface waves.

We choose a selection of sources that act as part of the integration boundary when applying equations 5 and 6; see the areas of green squares in Figure 1. Although this part of the boundary might not contain all sources required to construct all scattered events, in the following we show that it still is suitable to construct the dominant scattering events observed in the data set.

Halliday and Curtis (2009) show that the results of interferometry for scattered surface-wave recovery can vary greatly depending on source geometries and the type of interferometry applied. For correlation-type interferometry, we require sources that enclose the virtual source-receiver pair (or with limited geometries, the sources should be located outside the virtual source-receiver pairs). For convolution-type interferometry, we require sources enclosing only one of the receivers (or with limited geometry, the sources should be located between the virtual source-receiver pairs). Provided that we choose sources in this way, we find that the convolution-type interferometric estimates are reliable. In Appendix A, we include a further discussion on the selection of sources in light of the stationary-phase analysis presented by Halliday and Curtis (2009). In this discussion, we explain how, by applying interferometry using the available limited source geometries, we can expect to reconstruct the physical scattered surface waves.

We now apply interferometry to estimate the scattered surface waves in the gather in Figure 3c. The geometries used are shown in Figure 4a and b for correlation-type interferometry and convolution-type interferometry, respectively. We find that results are good when we choose a five by nine patch of sources to be the boundary sources for interferometry. Such a distribution of sources reduces the artifacts seen in the interferometric results (we discuss this in more detail in Appendix A). Note that a fully enclosing boundary of sources could have been constructed from the geometry in Figure 2. However, due to the assumption in equations 1–6 (that the boundary has a large radius), this introduces strong artifacts into the results that are not seen when using the limited patch of sources.

As a rule of thumb, we choose sources to be 75 m outside (for correlation) or inside (for convolution) the virtual source. We expect to be able to estimate scattered surface waves due to heterogeneities lying to the right of the dashed gray lines in Figure 4a and b. Note that we do not expect to estimate the waves between the patch of sources and the virtual sources, this is due to the isolation of the direct surface waves between these locations prior to applying interferometry. Although this limits our ability to recover all of the scattered surface waves, later we show that it is adequate to recover many of the scattered events seen in this data set.

The processing sequence to generate the interferometric gathers is as follows. At the virtual source location ($\mathbf{r}_A$), we sort the data into a common-receiver gather containing the isolated direct waves, $G_{33}^{\mathrm{d}}(\mathbf{r}_A,\mathbf{r}_S)$ in equations 5 and 6, between each boundary source and the virtual receiver, and for every other receiver of interest ($\mathbf{r}_B$) we sort the data into a common-receiver gather containing the isolated scattered (and body) waves, $G_{33}^{\mathrm{sc}}(\mathbf{r}_B,\mathbf{r}_S)$ in equations 5 and 6. Because $\mathbf{r}_A$ is the virtual source position, we fix this as the reference trace, and for all other receivers $\mathbf{r}_B$, we crosscorrelate (or crossconvolve) the two common-receiver gathers and sum the resulting traces, resulting in estimates of the scattered waves between a virtual source at $\mathbf{r}_A$ and all other receivers $\mathbf{r}_B$.

For correlation-type interferometry, we use the source geometries illustrated in Figure 4a, with the resulting scattered surface-wave estimate shown in Figure 5a. For convolution-type interferometry, we use the source geometries illustrated in Figure 4b, with the resulting scattered surface-wave estimate shown in Figure 5b. In Figure 5c, we show the data from the actual source (with the direct ground roll removed, as shown in Figure 3c). Comparing the results, it is clear that both correlation-type interferometry and convolution-type interferometry estimate many of the dominant scattered surface-wave events (for example, the dominant scatterer in the center of the gather, and other weaker scattering events at [400 m, 2.6 s]). We do expect losses due to attenuation to affect the correlation-type estimates, but because we consider sources that are close to the pair of receivers, these losses are minimal.

However, we can identify subtle differences between the plots. At [600 m, 2 s], there is an apex of a weak hyperbolic event in the convolution estimate that is not present in the correlation estimate. At [300 m, 2.3 s], the flank of the same hyperbolic event can be seen on the convolution estimate and the real data, but not in the correlation estimate. There are also subtle differences in phase and amplitude between the estimates made using correlation and convolution; this is because we approximate exact seismic interferometry when applying equations 5 and 6.

As the final part of our comparison, we consider the adaptive subtraction of these scattered surface-wave estimates from the real data. Here we require the virtual-source receiver to be close to a real source position. Ideally, the virtual-source receiver and the real source would be very close together (e.g., within the Fresnel zone of the other); however, larger offsets might be partially accounted for

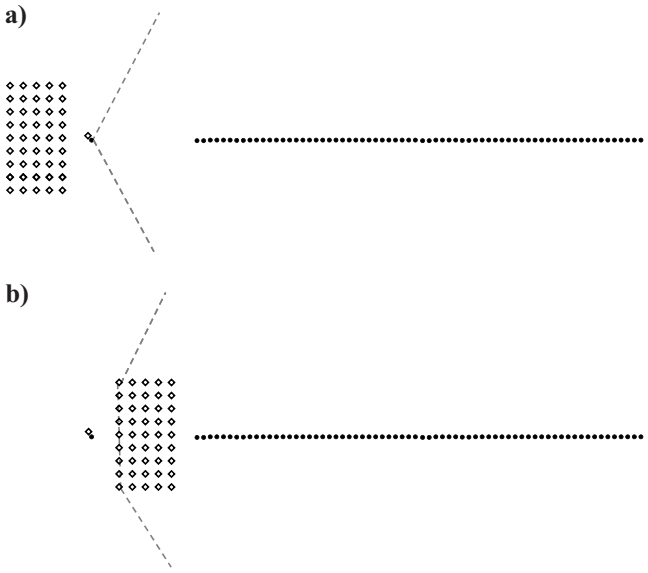

Figure 4. Geometries used to create scattering estimates in Figure 5. (a) Geometries for correlation-type interferometry and (b) geometries for convolution-type interferometry. Circles indicate receivers; diamonds indicate sources. The virtual source-real source pair is indicated by the neighboring circle and diamond, respectively. We expect to be able to estimate waves scattered by heterogeneities to the right of the gray dashed lines.

by the use of adaptive filtering. Because this data set is so well sampled, this distance is not an issue; however, this could be important when applying the method to other, less well sampled, data sets.

To perform the adaptive subtraction, we find some matching filter **f** that minimizes the difference between the real data (without the direct ground roll) $\mathbf{G}^{nd}$ and the estimated scattered surface waves $\mathbf{G}^{sc}$. In other words, we solve the following minimization problem for **f**:

$$\min_{\mathbf{f}} \|\mathbf{G}^{nd} - \mathbf{f}\mathbf{G}^{sc}\|. \tag{7}$$

In the following, we solve equation 7 in overlapping 2D windows (width 5 traces, length 0.25 s) using iterative least squares with a conjugate gradient algorithm to design 2D matching filters (with a maximum spatial lag of ± 2 traces and a maximum time lag of ± 5 samples; for more on adaptive filtering, see Claerbout, 2004). The scatterer-free seismic data $\mathbf{G}^{nsd}$ then are generated using

$$\mathbf{G}^{nsd} = \mathbf{G}^{nd} - \mathbf{f}\mathbf{G}^{sc}. \tag{8}$$

Later in this study, we wish to remove the scattered waves while preserving the direct ground roll (so that the resulting scatterer-free data can be used in a conventional seismic processing flow). To do this, we modify equation 8 so that the filtered data are subtracted from the full raw gather **G** to give the raw data without scattered surface waves,

$$\mathbf{G}^{nsc} = \mathbf{G} - \mathbf{f}\mathbf{G}^{sc}, \tag{9}$$

where $\mathbf{G}^{nsc}$ represents the raw data without scattered surface waves but with the direct surface waves intact.

We use this least-squares approach to match the scattered estimates in Figure 5a and b to the data shown in Figure 3c, and subtract the filtered estimates using equation 8. These results are shown in Figure 6a and b, again showing the data from Figure 3c for comparison in Figure 6c. We have used the same filter parameters for each adaptive subtraction, and both estimates give a similar result after this subtraction. It is likely that the adaptive filter accounts for the differences seen between the estimates in Figure 5a and b. Note that there are some near-horizontal events remaining in both gathers after adaptive subtraction of the estimated scattered ground roll (e.g., about 1.75 s). These could be interpreted as reflection events; however, it is more likely that these are crossline scattered waves that

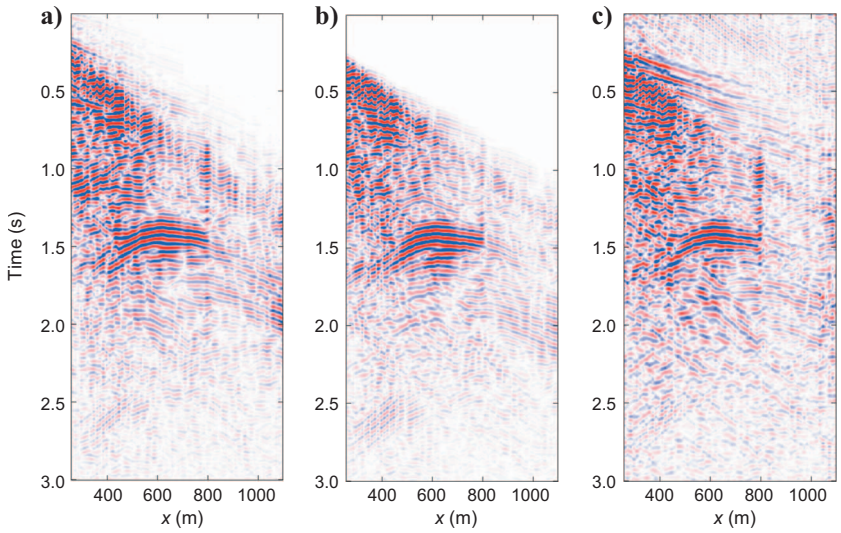

Figure 5. Interferometric estimates using (a) correlation-type interferometry and (b) convolution-type interferometry. (c) The data from Figure 3c is shown for comparison.

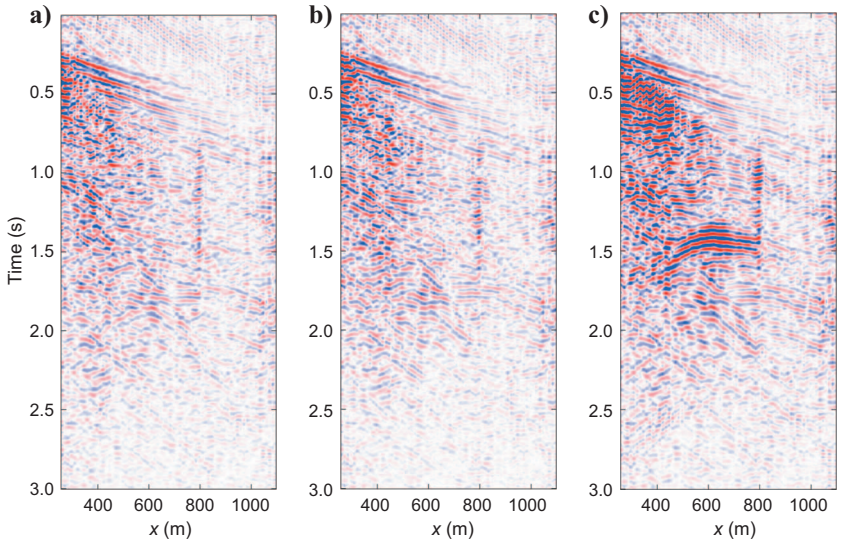

Figure 6. (a, b) Adaptive subtraction of interferometric estimates shown in Figure 5a and b from the data shown in Figure 5c. (c) The data from Figure 3c is shown for comparison.

have not been estimated by interferometry (for example, they might lie outside the regions indicated in Figure 4).

Although the results using convolution are expected to be better than those using correlation, one drawback of the convolution method is that we cannot make convolution estimates at short offsets because we require a gap for the boundary sources. In the following, we illustrate that by filling this gap using the correlation approach, it is possible to create scattered surface-wave estimates for the whole gather, preparing the data for conventional processing techniques.

We use crosscorrelation up to a source-receiver offset of 300 m, and beyond 300 m we use crossconvolution. We also split the data into positive and negative offsets because we require different sources when applying interferometry to positive and negative offsets. A schematic of the combination of geometries is shown in Figure 7. We estimate the scattering using the same process as above and adaptively subtract these estimates from the full wavefield using equations 7 and 9. We preserve the direct ground roll in these estimates so that it can be removed using existing methods (e.g., *f*-*k* or *f*-*x* methods), which also might remove any residual in-line scattered waves.

In Figure 8 and Figure 9, we show two gathers (a) before, and (b) after, the application of the interferometric method, along with (c) the removed scattered ground roll. These examples illustrate the removal of scattered ground roll while preserving the direct ground roll. We use convolution-type interferometry where possible because, as discussed in this section and in Appendix A, we previously identified that this approach is less sensitive to nonphysical arrivals and attenuation. Although we have not observed a large difference between the crosscorrelation and crossconvolution approaches in this case, it might be that different scatterer distributions are more susceptible to these changes. In Figure 10a-c, we show the equivalent *f*-*k* plots corresponding to Figure 8a-c, respectively. In Figure 10d-f, we show the plots corresponding to Figure 9a-c, respectively. These *f*-*k* plots illustrate the operation of the interferometric method inside the pass zone of a conventional *f*-*k* filter.

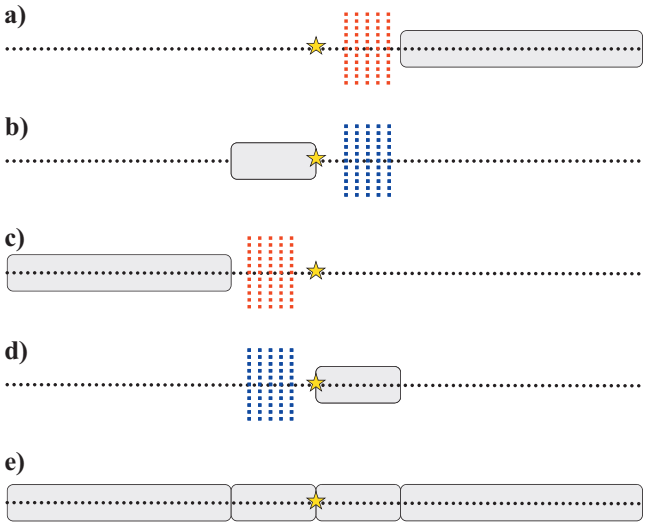

Figure 7. Sketch showing the application of interferometry for a full gather. Red and blue squares indicate sources used for convolution and correlation, respectively; the yellow star is the position of the real and virtual sources, and black dots indicate the receiver line. Shaded boxes indicate the receivers considered in each step. (a) Convolution for forward offsets, (b) correlation for backward offsets, (c) convolution for backward offsets, and (d) correlation for forward offsets. Finally, (e) shows the combination of the four shaded regions in (a) through (d).

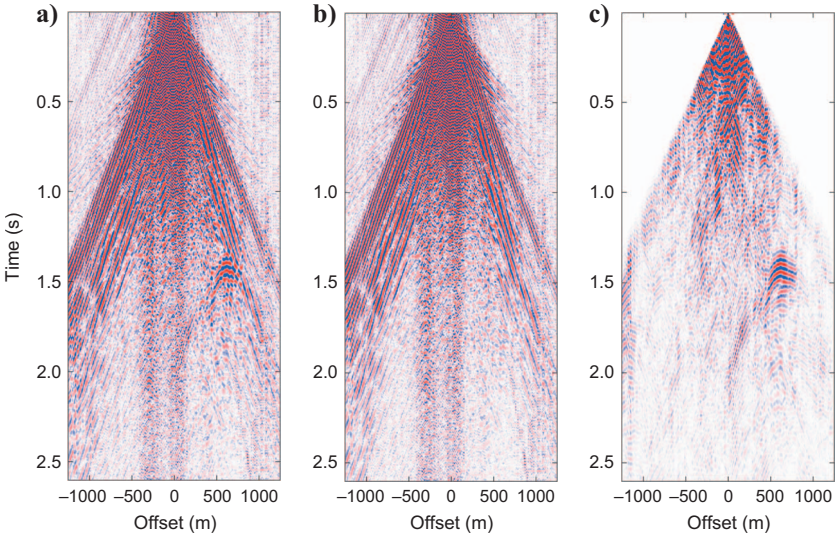

Figure 8. Example of interferometric ground-roll removal applied to a full gather while preserving the direct ground roll. (a) Raw data, (b) results of interferometric ground-roll removal, and (c) the subtracted (scattered) ground roll.

To illustrate the method further, we consider digital group forming (DGF) using the shot gathers shown in Figure 9a and b, considering all eight receiver lines shown in Figure 2. Digital group forming is a process that allows the application of optimally designed noise-attenuation filters to single-sensor data before group forming, instead of stacking recording arrays in the field (as in conventional array-based acquisition). Figure 11a illustrates the data after DGF in the time-offset domain for the data without the application of interferometric ground-roll removal, and Figure 11b shows the equivalent plot with the application of interferometric ground-roll removal. A $t^{1.5}$ gain and a 50-Hz low-pass filter are applied to the data before plotting. Clear improvements can be seen within the noise cone, especially at about 1.2 s where the strong reflection event has greater continuity across the noise cone. This is illustrated further in Figure 12, where zoomed sections of the gather are shown (from 0.9 to 1.7 s). In Figure 11 and Figure 12, the dotted ovals indicate regions where the scattered noise is particularly problematic.

DISCUSSION

Our results indicate that interferometric ground-roll removal could be a solution to the problem of crossline scattered ground roll. As is typical of single-sensor data, it is difficult to identify strong reflection events in the raw data, although some reflection events can be observed in the digital group-formed data and the interferometric approach appears to improve the continuity of these reflection events across the noise cone. In the timescale of this study, it was not possible to process the whole test line up to stack. However, to test whether reflection energy is at all attenuated by our method, we have repeated the process involved in creating Figure 6b but with the inclusion of three synthetic reflection events in all data used in the processing. We model three P-wave reflections from horizontal planar reflectors at depths of 1500, 2000, and 3000 m, respectively, using a constant P-wave velocity of 3000 m/s.

In Figure 13, we show (a) the raw data with synthetic reflections, (b) the interferometric estimate, (c) the data after *f-k* filtering of the direct ground roll and adaptive subtraction of the interferometric es-

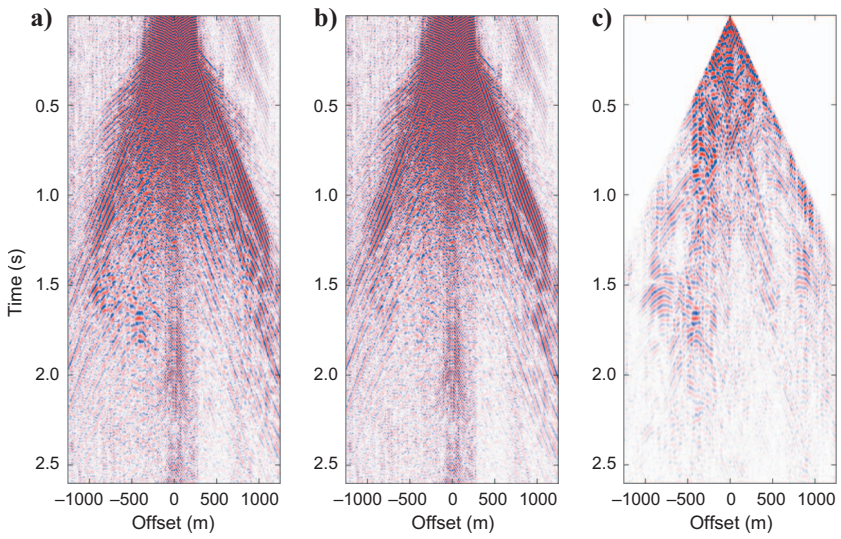

Figure 9. Example of interferometric ground-roll removal applied to a full gather while preserving the direct ground roll. (a) Raw data, (b) results of interferometric ground-roll removal, and (c) the subtracted (scattered) ground roll.

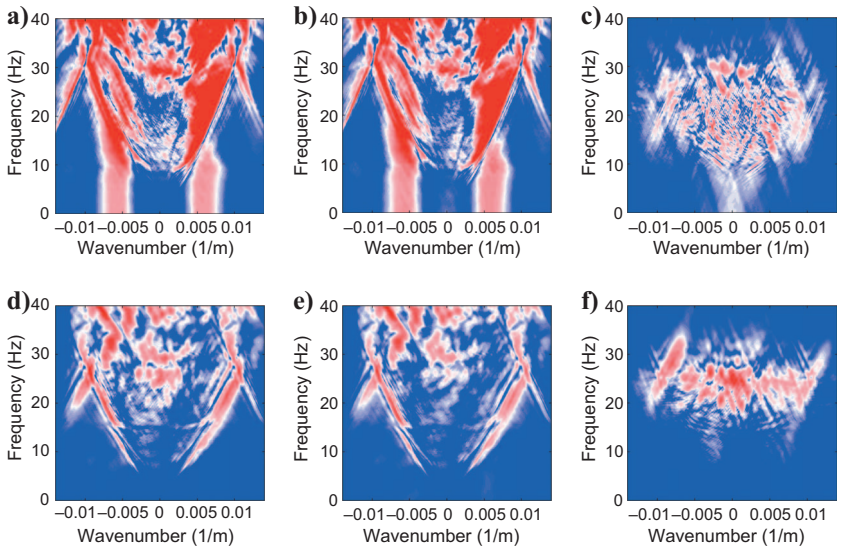

Figure 10. Frequency-wavenumber plots corresponding to Figure 8a-c: (a-c), respectively; and those corresponding to Figure 9a-c: (d-f), respectively.

timate, and (d) the data in Figure 13c after subtraction of the original modeled reflections. The lack of a strong residual in Figure 13d suggests that these strong synthetic reflection events have been preserved during interferometric ground-roll removal. There is a small residual, but the residual is not present in the interferometric estimate (Figure 13b). It is therefore likely that the residual is a signal-processing artifact from the adaptive subtraction of the scattered surface waves, instead of an artifact introduced by interferometry.

The geometries in the test data set appear to be suitable to estimate the scattering observed here. However, this is not a typical source geometry, and it might be that a change of geometry is required for the interferometric method to be fully applied in exploration and production. Typically, source lines are coarsely spaced (Vermeer, 2002), and the application of interferometry might not be as successful (for example, we might have to consider interpolating sources over a significant distance). There is scope for further work to determine if the method can be applied to conventional data sets and to find an optimal geometry for the application of the method. For example, it might be possible to use near-surface characterization to choose an appropriate geometry for scattered-wave recovery.

There are other advantages to having estimates of the scattered waves, even if it is not possible to adaptively subtract them from all source gathers (in typical 3D land data sets, it is unlikely that every source will have a neighboring receiver). For example, interferometric estimates could help to characterize near-surface scattering: because the estimates contain predominantly scattered waves, it might be relatively easy to distinguish which arrivals are scattering events. In addition, the estimates of scattered waves might also be used in near-surface imaging algorithms (e.g., Campman and Riyanti, 2007; Kaslilar, 2007); hence a combination of our method and inverse-scattering-based ground-roll removal could bear fruit in the future.

Recent advances have also shown that interferometry can be adapted so that crosscorrelation is replaced with deconvolution, an approach that also might account for intrinsic attenuation. Multidimensional deconvolution (MDD) is proposed for seismic interferometry by Wapenaar et al. (2008a and 2008b), and it is a method that uses arrays of receivers and a matrix inversion to extract array-receiver (or array-array) Green's functions. It is expected that MDD is less sensitive to nonuniform source distributions and to the presence of attenuation. In addition, Vasconcelos and Snieder (2008) consider the use of deconvolution interferometry applied to direct and scattered wavefields. Vasconcelos et al. (2008) discuss the use of deconvolution interferometry to predict and subtract scattered surface waves, suggesting that the deconvolution version of the method also could be a powerful tool in predicting and subtracting scattered ground roll. Curtis and Halliday (2010b) show that a double-integral form of interferometry can be used to estimate the wavefield between a source and a receiver, and this approach may also be used to predict direct and scattered ground roll.

Several opportunities also exist to improve the interferometric estimates. For example, in the presence of directional bias in recorded energy (e.g. due to source line sparsity), directional balancing algorithms exist that allow for (correlation-type) interferometric Green's function estimates to be altered to more closely resemble those from isotropic point sources, and algorithms have been proposed that remove nonphysical arrivals (Wapenaar et al., 2008b; Van der Neut and Bakulin, 2009; Curtis and Halliday, 2010a). It is also possible to apply damping factors to account for the presence of attenuation when using correlation-type interferometry (Draganov et al., 2010).

Finally, in the future we might consider other adaptive subtraction schemes, such as pattern matching (Guitton et al., 2007) or the use of 3D (x, y, t) filters (Claerbout, 1998). Nevertheless, this work already demonstrates the ability of interferometry to predict and subtract scattered ground roll without adapting the interferometric processing schemes (which might make the method more computationally expensive), or without more advanced adaptive subtraction schemes.

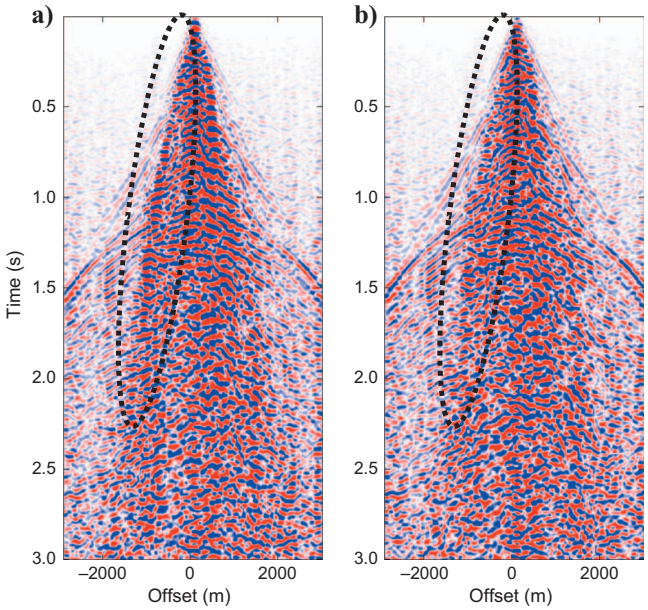

Figure 11. Results of digital group forming (DGF) for the source gather shown in Figure 9 (using the eight neighboring receiver lines illustrated in Figure 2). (a) DGF result without the application of interferometric ground-roll removal, and (b) DGF result using the data after application of interferometric ground-roll removal. The dotted ovals indicate the region of the gather where strong scattered noise is particularly problematic.

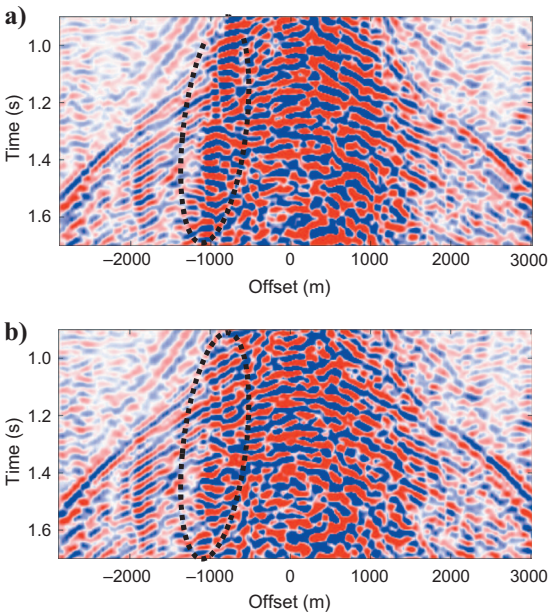

Figure 12. Zoomed portions of Figure 11a and b, respectively. The dotted ovals indicate the region of the gather where strong scattered noise is particularly problematic.

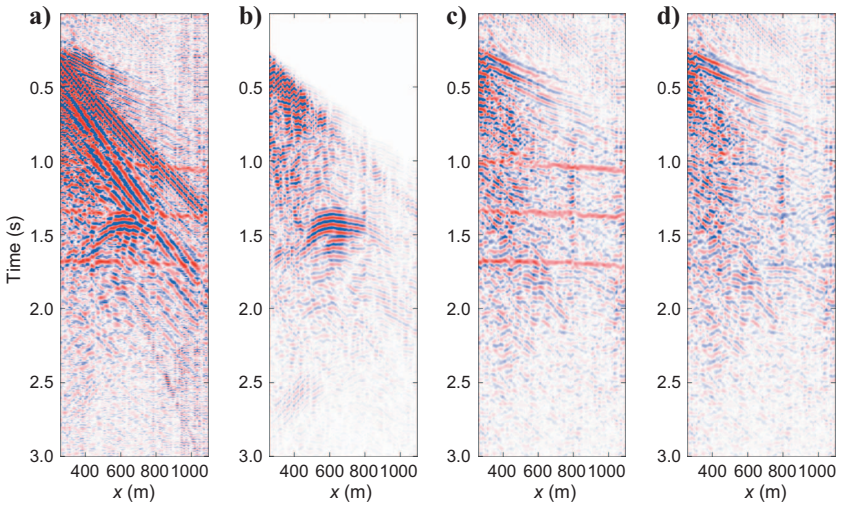

Figure 13. Results for convolution interferometry after introducing three synthetic reflections. (a) Raw gather, (b) interferometric estimate of the scattered ground roll, (c) result of f-k filtering of the direct ground-roll and interferometric ground-roll removal, and (d) residual after subtraction of modeled reflections.

CONCLUSIONS

We have shown that scattered surface waves can be successfully predicted using both correlation-type and convolution-type interferometric approaches. These interferometric estimates are consistent with previous work on surface-wave interferometry, and for the first time we have used both correlation-type and convolution-type interferometric estimates of scattered surface waves to attenuate scattered ground roll from single-sensor land seismic data.

Our results illustrate the ability of this new method to successfully suppress scattered ground-roll energy, allowing for the further processing of better quality data. We have also shown that better continuity of reflection events in group-formed data results from the application of the method. Applying the method to data with synthetic reflections added to the raw data suggests that the method does not attenuate reflection data significantly. Future work on the method will include further processing to assess the effect of the method on stacked seismic data. The method has the potential to form a vital part of the processing sequence for land seismic data in the same way that surface-related multiple elimination has become a vital part of the processing sequence for marine data.

The data set geometry that we consider is not typical of a land seismic survey; it might be that a change in survey design is required to fully apply the method in exploration and production. Further research must be undertaken also to investigate the effect of different acquisition geometries, and to assess the method in regions with different near-surface scattering characteristics.

ACKNOWLEDGMENTS

We thank Apache Egypt and WesternGeco for permission to publish the data. We acknowledge the support of the Scottish Funding Council for the Joint Research Institute with Heriot-Watt University, which is part of the Edinburgh Research Partnership in Engineering and Mathematics (ERPem). Deyan Draganov, Xander Campman, and two anonymous reviewers are thanked for their comments, which helped to improve the manuscript.

APPENDIX A

DISCUSSION OF STATIONARY PHASE, SOURCE POSITION, AND NONPHYSICAL ARRIVALS

We now consider the distribution of stationary-phase regions for scattered surface-wave recovery in relation to the source geometries available in the test data set. For the estimation of a single-scattered surface wave by correlation-type interferometry, the stationary regions lie on the extension of the paths between each receiver and the scatterer (Halliday and Curtis, 2009). In Figure A-1a, we show a sketch with two receiver positions ($\mathbf{r}_A$ and $\mathbf{r}_B$) and a single scatterer (sc); the distribution of sources we consider is illustrated by the blue shaded area. The stationary-phase regions for the single-scattered surface wave propagating from $\mathbf{r}_A$ to $\mathbf{r}_B$ via sc are indicated by the yellow shaded areas SR_{P1} and SR_{NP}. Sources in these regions will contribute arrivals to the interferometric estimate that stack constructively in the application of equation 5.

For a source in the stationary region SR_{P1}, the crosscorrelation removes the common path from the waves observed at each receiver. In this case, the common path is the path between the source in SR_{P1} and the virtual source $\mathbf{r}_A$. Removing this path results in the observation of the scattered wave at $\mathbf{r}_B$ as if it had been excited by a source at $\mathbf{r}_A$; i.e., this contributes a physical arrival. However, for a source located within the stationary region SR_{NP}, the common path is the path between the source and the scatterer. The resulting arrival observed at $\mathbf{r}_B$ has a phase that is the same as the phase difference of a wave propagating between the scatterer (sc) and each receiver ($\mathbf{r}_A$ and $\mathbf{r}_B$). This arrival does not correspond to the physical scattered wave and results in a nonphysical term. For the off-line scatterer considered here, we observe that this nonphysical stationary region does not coincide with the source distribution. Therefore, if we choose sources for interferometry that lie to the left of receiver $\mathbf{r}_A$ (the virtual source), and coincide with the region SR_{P1}, we can be confident that we can estimate off-line scattered waves while mitigating for some of the nonphysical arrivals that might be introduced.

In Figure A-1b, we show a similar sketch for an in-line scatterer. The physical stationary-phase region again is located to the left of receiver $\mathbf{r}_A$, but the nonphysical stationary-phase region also coincides with the source distribution in this case. Hence, by following the observations of our previous work, we can attempt to mitigate for nonphysical scattered arrivals, but we also can select sources from which we can expect to construct scattered surface waves.

A similar analysis for the convolution case is simpler because in this case (and in the specific configurations shown), the stationary phase region SR_{P2} is located between the scatterer and the receiver, and there is *only* a physical contribution. In both of our sketches, the source coverage coincides with the stationary-phase region for the scattered wave when applying convolution-type interferometry.

By applying intuition from our previous stationary-phase analysis, using the limited source geometries available, we have identified that we can expect to reconstruct the physical scattered surface waves, but we can also choose sources so that we limit the introduction of nonphysical arrivals. Vasconcelos et al. (2009) identify simi-

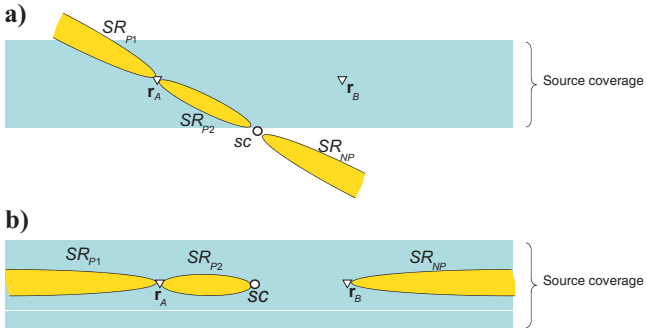

Figure A-1. Sketch geometry showing the source distribution (blue shaded area), two receivers (triangles), a single scatterer (circle), and various stationary-phase regions discussed in Appendix A for (a) an off-line scatterer and (b) an in-line scatterer.

lar nonphysical arrivals for acoustic waves. They propose to limit the choice of boundary sources so that nonphysical arrivals do not appear in their interferometric estimates in a similar fashion to the case shown in our sketches.

REFERENCES

Bakulin, A., and R. Calvert, 2006, The virtual source method: Theory and case study: Geophysics, **71**, no. 4, SI139–SI150.

Blonk, B., and G. C. Herman, 1996, Removal of scattered surface waves using multicomponent seismic data: Geophysics, **61**, 1483–1488.

Blonk, B., G. C. Herman, and G. G. Drijkoningen, 1995, An elastodynamic inverse scattering method for removing scattered surface waves from field data: Geophysics, **60**, 1897–1905.

Campman, X., and C. D. Riyanti, 2007, Non-linear inversion of scattered seismic surface waves: Geophysical Journal International, **171**, 1118–1125.

Chávez-García, F. J., and F. Luzón, 2005, On the correlation of seismic microtremors: Journal of Geophysical Research, **110**, B11313.

Claerbout, J. F., 1998, Multidimensional recursive filters via a helix: Geophysics, **63**, 1–13.

———, 2004, Earth soundings analysis: Processing versus inversion, http://sepwww.stanford.edu/sep/prof/, accessed 2 February 2005.

Curtis, A., P. Gerstoft, H. Sato, R. Snieder, and K. Wapenaar, 2006, Seismic interferometry — Turning noise into signal: The Leading Edge, **25**, 1082–1092.

Curtis, A., and D. F. Halliday, 2010a, Directional balancing for seismic and general wavefield interferometry: Geophysics, **75**, no. 1, SA1–SA14.

Curtis, A., and D. F. Halliday, 2010b, Source-receiver wave-field interferometry: Physical Review E, **81**.

Dong, S., R. He, and G. Schuster, 2006, Interferometric prediction and least-squares subtraction of surface waves: 76th Annual International Meeting, SEG, Expanded Abstracts, 2783–2786.

Draganov, D., R. Ghose, E. Ruigrok, J. Thorbecke, and K. Wapenaar, 2010, Seismic interferometry, intrinsic losses and Q-estimation: Geophysical Prospecting, **58**, in press.

Ernst, F., G. C. Herman, and B. Blonk, 2002a, Reduction of near-surface scattering effects in seismic data: The Leading Edge, **17**, 759–764.

Ernst, F., G. C. Herman, and A. Ditzel, 2002b, Removal of scattered guided waves from seismic data: Geophysics, **67**, 1240–1248.

Gerstoft, P., K. G. Sabra, P. Roux, W. A. Kuperman, and M. C. Fehler, 2006, Green's functions extraction and surface-wave tomography from microseisms in southern California: Geophysics, **71**, no. 4, SI23–SI31.

Guitton, A., B. Kaelin, and B. Biondi, 2007, Least-squares attenuation of reverse-time-migration artifacts: Geophysics, **72**, no. 1, S19–S23.

Halliday, D., and A. Curtis, 2008, Seismic interferometry, surface waves and source distribution: Geophysical Journal International, **175**, 1067–1087.

———, 2009, Seismic interferometry of scattered surface waves in attenuative media: Geophysical Journal International, **178**, 419–446.

Halliday, D., A. Curtis, and E. Kragh, 2008, Seismic surface waves in a suburban environment — Active and passive interferometric methods: The Leading Edge, **27**, 210–218.

Halliday, D., A. Curtis, J. O. A. Robertsson, and D.-J. van Manen, 2007, Interferometric surface-wave isolation and removal: Geophysics, **72**, no. 5, A69–A73.

Herman, G. C., and C. Perkins, 2006, Predictive removal of scattered noise: Geophysics, **71**, no. 2, V41–V49.

Kaslilar, A., 2007, Inverse scattering of surface waves: Imaging of near-surface heterogeneities: Geophysical Journal International, **171**, 352–367.

Mehta, K., A. Bakulin, J. Sheiman, R. Calvert, and R. Snieder, 2007, Improving the virtual source method by wavefield separation: Geophysics, **72**, no. 4, V79–V86.

Özbek, A., 2000, Adaptive beamforming with generalized linear constraints: 70th Annual International Meeting, SEG, Expanded Abstracts, 2081–2084.

Poletto, F., and B. Farina, 2008, Synthesis of a virtual reflector by processing recorded seismic signals: 70th Annual Conference and Exhibition, EAGE, Extended Abstracts.

Poletto, F., and K. Wapenaar, 2009, Virtual reflector representation theorem (acoustic medium): Journal of the Acoustical Society of America, **125**, no. 4, EL111–EL116.

Regone, C. J., 1998, Suppression of coherent noise in 3-D seismology: The Leading Edge, **17**, no. 11, 1584–1589.

Shapiro, N., and M. Campillo, 2004, Emergence of broadband Rayleigh waves from correlations of the ambient seismic noise: Geophysical Research Letters, **31**, L07614.

Shapiro, N., M. Campillo, L. Stehly, and M. Ritzwoller, 2005, High-resolution surface-wave tomography from ambient seismic noise: Science, **307**, 1615–1617.

Slob, E., D. Draganov, and K. Wapenaar, 2007, Interferometric electromagnetic Green's functions representations using propagation invariants: Geophysical Journal International, **169**, 60–80.

Slob, E., and K. Wapenaar, 2007, Electromagnetic Green's functions retrieval by cross-correlation and cross-convolution in media with losses: Geophysical Research Letters, **34**, L05307.

Snieder, R., K. van Wijk, M. Haney, and R. Calvert, 2008, The cancellation of spurious arrivals in Green's function extraction and the generalized optical theorem: Physical Review E, **78**, 036606.

Van der Neut, J., and A. Bakulin, 2009, Estimating and correcting the amplitude radiation pattern of a virtual source: Geophysics, **74**, no. 2, SI27–SI36.

Van Manen, D.-J., J. O. A. Robertsson, and A. Curtis, 2005, Modeling of wave propagation in inhomogeneous media: Physical Review Letters, **94**, 164301.

Van Manen, D.-J., A. Curtis and J. O. Robertsson, 2006, Interferometric modelling of wave propagation in inhomogeneous elastic media using time-reversal and reciprocity: Geophysics, **71**, no. 4, S147–S160.

Vasconcelos, I., J. Gaiser, A. Calvert, and C. Calderón-Macías, 2008, Retrieval and suppression of surface waves using interferometry by correlation and by deconvolution: 78th Annual International Meeting, SEG, Expanded Abstracts, 2566–2569.

Vasconcelos, I., and R. Snieder, 2008, Interferometry by deconvolution: Part 1 — Theory for acoustic waves and numerical examples: Geophysics, **73**, no. 3, S115–S128.

Vasconcelos, I., R. Snieder, and H. Douma, 2009, Representation theorems and Green's function retrieval for scattering in acoustic media: Physical Review E, **80**, 036605.

Vermeer, G., 2002, 3D Seismic survey design: SEG Geophysical Reference Series 12.

Wapenaar, K., 2003, Synthesis of an inhomogeneous medium from its acoustic transmission response: Geophysics, **68**, 1756–1759.

———, 2004, Retrieving the elastodynamic Green's function of an arbitrary inhomogeneous medium by cross correlation: Physical Review Letters, **93**, 254301.

———, 2007, General representations for wavefield modeling and inversion in geophysics: Geophysics, **72**, no. 5, SM5–SM17.

Wapenaar, K., and J. Fokkema, 2006, Green's function representations for seismic interferometry: Geophysics, **71**, no. 4, SI33–SI44.

Wapenaar, K., E. Slob, and R. Snieder, 2006, Unified Green's function retrieval by cross-correlation: Physical Review Letters, **97**, 234301.

———, 2008a, Seismic and electromagnetic controlled-source interferometry in dissipative media: Geophysical Prospecting, **56**, 419–434.

Wapenaar, K., J. van der Neut, and E. Ruigrok, 2008b, Passive seismic interferometry by multidimensional deconvolution: Geophysics, **73**, no. 6, A51–A56.

Yilmaz, Ö., 2001, Seismic data analysis: Processing, inversion and interpretation of seismic data: SEG Investigations in Geophysics 10.